# Supplementary information

## Observation of a robust catalyst support based on metallic glass for large current-density water electrolysis

*Mengqi Pan[a,b], Heyang Feng[a], Ziyong Zhang[a], Meng Gao[a,b], Lei Lei[c], Degao Wang[c] Guowei Li[a]\*, Juntao Huo[a,b]\*, Jun-Qiang Wang[a,b]\**

a.  CAS Key Laboratory of Magnetic Materials and Devices, and Zhejiang Province Key Laboratory of Magnetic Materials and Application Technology, Ningbo Institute of Materials Technology and Engineering, Chinese Academy of Sciences, Ningbo, China

b.  Center of Materials Science and Optoelectronics Engineering, University of Chinese Academy of Sciences, Beijing, China

c.  Zhejiang Key Laboratory of Data-Driven High-Safety Energy Materials and Applications Ningbo Institute of Materials Technology and Engineering, Chinese Academy of Sciences, Ningbo, China

Email: liguowei@nimte.ac.cn; huojuntao@nimte.ac.cn; jqwang@nimte.ac.cn;

**Materials preparation**

Fe, Co, Ni, Zr, and Pt (>99 wt%) were precisely formulated according to established ratios. An alloy ingot of $Fe_{70-x}Co_{10}Ni_{10}Zr_{10}Pt_x$, with a homogeneous composition, was then prepared using the melt spinning technique, conducted in an environment protected by high-purity argon (Ar) atmosphere. Utilizing the single-roll rapid quenching technique, the molten alloy ingot was expeditiously sprayed onto a copper roll, rotating at a high tangential speed of 45 m s$^{-1}$, to fabricate a metallic glass sample measuring 5 meters in length, 1 mm in width, and 40-60 μm in thickness. The produced ribbons were sectioned into 3 cm long samples, streamlining electrode fabrication. These segments were then naturally corroded in 2 M $H_2SO_4$ solution, predominantly through dealloying, to achieve a nanoporous morphology on their surfaces to obtain platinum loaded on MG support catalysts (Pt/MG). Subsequently, the catalysts were cleansed using deionized water and anhydrous alcohol.

The comparative sample Pt/C @ MG was prepared using the following method: The MG support (without Pt) was immersed in a 2M $H_2SO_4$ solution for 1.5 hours, leading to the creation of a highly porous Pt0/MG structure. To prepare the Pt/C @ MG sample, 5 mg of Pt/C (20 wt%) and 50 μL of Nafion solution were mixed with 1000 μL of anhydrous ethanol. This mixture was sonicated for 30 minutes to ensure uniform dispersion. Then, 20 μL of this mixture was carefully applied to the Pt0/MG material, distributing 10 μL on each side. The designated loading area for the Pt/C was 0.32 cm², corresponding to a loading density of 0.2976 mg cm$^{-2}$. Following the application, the Pt/C @ MG composite was dried and subsequently employed as the working electrode.

**Materials characterization**

The phase structures of the catalysts were characterized by X-ray diffraction (XRD, Bruker, D8 ADVANCE). The morphology of the catalysts was observed by scanning electron microscopy (SEM, Zeiss, G300). The surface and cross-sectional structures of both as-spun Pt$x$ and Pt$x$/MG catalysts, along with their elemental distribution, were analyzed using energy-dispersive X-ray spectroscopy (EDS) conducted with a transmission electron microscope (TEM, Talos F200x) and Double aberration-corrected transmission electron microscope (AC-TEM, Spectra 300). Additionally,

electron microscopy (TEM and SEM) was employed to examine the surface and cross-sections of the pristine and dealloyed ribbons. Surface and cross-section of the samples for TEM were prepared by ion thinning and focused ion beam (FIB) milling. The surface chemical states and binding energy of the samples were obtained through X-ray photoelectron spectroscopy (XPS, Kratos, Axis Ultra DLD) with calibration of peaks against impurity carbon (C $1s$ at 284.5 eV). The X-ray absorption spectra (XAS) measurements for the Pt $L_3$-edge were conducted in transmission mode (fluorescence mode) on the Laboratory-Based XAFS and XES Spectrometer (easyXAFS300+, USA). The energy was calibrated using corresponding metal foil as references. XANES and EXAFS data reduction and analysis were analyzed by Athena and Artemis software.

**Electrochemical measurement**

Electrochemical measurements were carried out at room temperature using an electrochemical workstation (Zahner Zennium) with a three-electrode system. The set up comprised a graphite rod as the counter electrode and an Ag/AgCl reference electrode, the latter containing a chloride ion concentration of 3.5 M. The size of the working electrode was 1 cm*0.1 cm*40 μm and the catalysts were tested in 1M KOH solution. The HER performance of Pt ribbon and Pt/C (20 wt.%, Johnson Matthey) catalysts were investigated for comparison. To maintain sample consistency, Pt/C was loaded onto the $Fe_{70}Co_{10}Ni_{10}Zr_{10}$ ribbon after 1.5 hours of dealloying (Pt/C @MG) with a loading of 0.179 mg cm$^{-2}$. The as-spun ribbons, Pt$x$/MG catalysts, and Pt ribbons were employed directly as working electrodes. Linear sweep voltammetry (LSV) measurements were conducted at a scan rate of 5 mV s$^{-1}$. The polarization curves from the LSV were normalized to the geometric area, with 90% iR compensation applied, and Tafel slopes were derived from these curves. Electrochemical impedance spectroscopy (EIS) analysis were conducted over a frequency range of 100 mHz to 100 kHz, with an amplitude setting of 5 mV. Additionally, the EIS measurements were carried out at a test potential of −0.3 V versus RHE in hydrogen evolution reaction (HER) and 0.3V in oxygen evolution reaction (OER). Stability tests were conducted via chronopotentiometry at a current density of −500 mA cm$^{-2}$, without iR compensation. For evaluating the electrochemical surface area (ECSA), cyclic

voltammetry (CV) measurements were performed in the non-Faradaic potential region at scan rates of 20, 40, 60, 80, 100, 120, 140, 160 mV s$^{-1}$, which facilitated the estimation of the sample's double-layer capacitance ($C_{dl}$). According to the relationship:

$$ECSA = C_{dl}/C_s \tag{1}$$

The $C_s = 40$ µF cm$^2$.

**Note S1**

The Faraday efficiency of the samples was calculated by the hydrogen collection method at current densities of 200 mA cm$^{-2}$, and the calculation formula is:

$$\eta = \frac{nmF}{It} \tag{2}$$

*n* (mol) is the mount of substance; *M* is the number of electrons transferred to create a H$_2$ (*m*=2 for HER); *F* is the Faraday's constant (96485 C mol$^{-1}$); *I* is the amount of current（A）; *t* is the response time (s).

**Note S2**

By estimating the quantity of hydrogen molecules precipitated per second from each active site at a given voltage, the turnover frequency (TOF) is ascertained, which facilitates the calculation of the sample's intrinsic catalytic activity. The formula for calculating TOF employed in this work is[1] :

$$TOF = \frac{\#total\ hydrogen\ turnovers}{\#active\ sites} \quad \text{or} \quad TOF = \frac{jAZ^{-1}F^{-1}N_A}{v_a \times A_{ECSA}} \tag{3}$$

*j* (mA cm$^{-2}$) is the current density based on the polarization curve; *A* is the geometric surface area of electrodes; *F* is the Faraday constant (96485.3 C mol$^{-1}$ ); *Z* is the molar number of the active materials (*Z*= 2 for HER); $N_A$ is Avogadro's constant $6.022 \times 10^{23} mol^{-1}$; $v_a$ is the amount of active sites on the surface of the electrode. Therefore, the total hydrogen turnover is calculated as:

$$\#total\ hydrogen\ turnovers = (j\frac{mA}{cm^{-2}})(\frac{1\ c\ s^{-1}}{1000mA})(\frac{1\ mol^{-1}e^{-1}}{96485.3\ c})(\frac{1\ mol\ H_2}{2mol\ e^{-1}}($$

$$\dfrac{6.022 \times 10^{23} molecules\ H_2}{1\ mol\ H_2})$$

$$= 3.12 \times 10^{15}\ H_2\ S^{-1}\ cm^{-2}\ per\ mA\ cm^{-2}$$

And:

$$v_a = \left( \dfrac{atomic \dfrac{number}{unit} cell}{\dfrac{volume}{unit} cell} \right)^{\frac{2}{3}}$$

(4)

The cell parameter of the nanocrystals is 3.9 Å, and there are four atoms per face-centered cubic (fcc) cell, and Pt is the active site.

So: $TOF_{Pt3/MG} = 2.5012 \times 10^{-3} j$

$TOF_{Pt5/MG} = 2.0973 \times 10^{-3} j$

Therefore, the TOF of the Pt3/MG at overpotentials of 50mV, 100mV, 150mV, 200mV are $TOF_{50} = 0.175\ H_2\ S^{-1}$, $TOF_{100} = 0.975\ H_2\ S^{-1}$, $TOF_{150} = 1.886\ H_2\ S^{-1}$, $TOF_{200} = 2.831\ H_2\ S^{-1}$. The TOF of the Pt5/MG at overpotentials of 50mV and 100mV, are $TOF_{50} = 0.522\ H_2\ S^{-1}$, $TOF_{100} = 2.053\ H_2\ S^{-1}$.

**DFT calculation**

First-principles calculation was performed using DMol[3] code in the Materials Studio package.[2] The Perdew-Burke-Ernzerhof (PBE) functional within the generalized gradient approximation (GGA) was used to describe the exchange-correlation effects. Using the effective core potentials (ECPs) to process the inner electrons of the metal, and DNP basis set that is a double numerical plus polarization was adopted.[3] The convergences of the energy, maximum force, and maximum displacement were confirmed as $2\times10^{-5}$ Ha, $4\times10^{-3}$ Ha Å$^{-3}$, and $8\times10^3$ Å, respectively. A $3\times3\times1$ Monkhorst-Pack grid was employed to execute the Brillouin-zone integrations.[4] The complete LST/QST and a mode-eigenvector following methods were employed to search these transition states (TSs) of all elementary re actions. The model of amorphous alloy was established based on the ratio of Fe: Ni: Co=4.8:1:1, which is consistent with the experimental approximation. The Pt (111) model was constructed with two metal atomic layers. Then the heterostructure of the two models is constructed, and the atoms in the bottom two layers were kept frozen while the remaining were allowed to relax during the slab calculations. A vacuum layer of 25 Å between periodically repeated slabs was set to avoid interactions among the slabs.

The hydrogen evolution reaction mechanism is expressed as:

$$^*\text{H} + \text{e}^- \rightarrow 1/2\ \text{H}_2 \tag{5}$$

The hydrogen adsorption energy on the catalyst surface is defined as:

$$\Delta E_{*\text{H}} = E_{*\text{H}} - E_* - 1/2\ E_{\text{H2}} \tag{6}$$

where $E_{*\text{H}}$, $E_*$, and $E_{\text{H2}}$ represent the energies of catalyst adsorbed with single H atom, isolated catalyst, and $\text{H}_2$ molecule, respectively.

The Gibbs free energy of hydrogen adsorption ($\Delta G_{*\text{H}}$) can be calculated by:

$$\Delta G_{*\text{H}} = \Delta E_{*\text{H}} + \Delta E_{\text{ZPE}} - T\Delta S \tag{7}$$

where $\Delta E_{\text{ZPE}}$ and $\Delta S$ represent the change in zero-point energy and entropy, respectively. T is the temperature of 298.15 K.
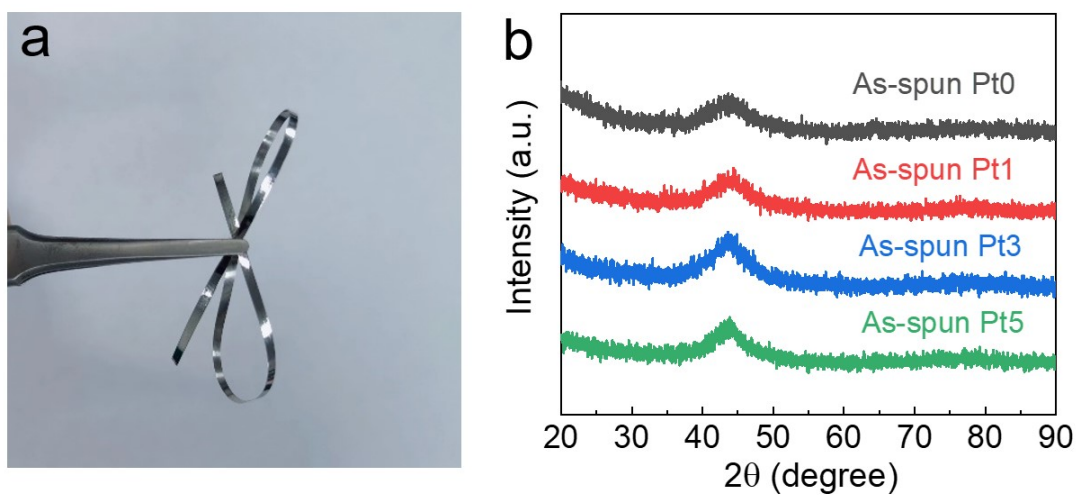
**Fig. S1** Structure of amorphous alloy precursors. (a) The image of the MG ribbon. (b) XRD patterns of the as-spun ribbons.

(The alloy precursors of $Fe_{70-x}Co_{10}Ni_{10}Zr_{10}Pt_x$ ($x$=0, 1, 3, 5) ribbons were metallic glass (MG ribbons), named as as-spun Pt$x$. The ribbons are flexible and have self-supporting performance as an electrocatalyst.
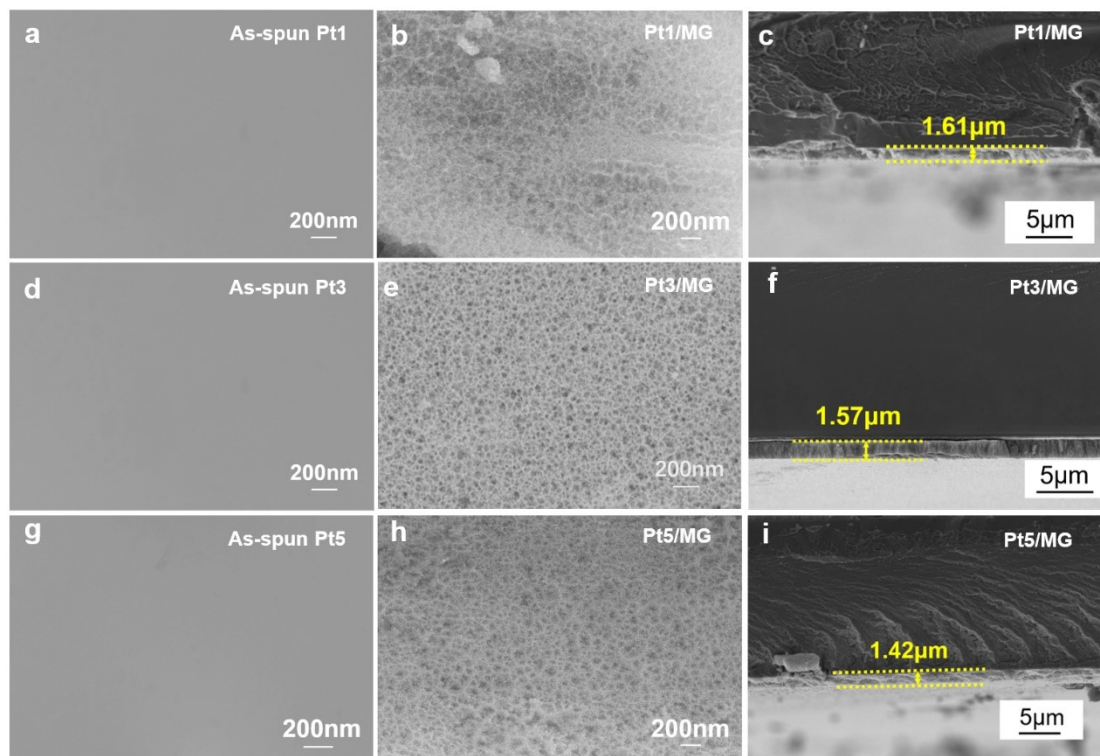
**Fig. S2** SEM structure and morphology of the as-spun Pt*x* ribbons and Pt*x*/MG catalysts. (a-c) The surface of the as-spun Pt1 ribbon, surface and cross-sectional morphology of Pt1/MG catalyst. (d-f) The surface of the as-spun Pt3 ribbon, surface and cross-sectional morphology of Pt3/MG catalyst. (g-i) The surface of the as-spun Pt5 ribbon, surface and cross-sectional morphology of Pt5/MG catalyst.
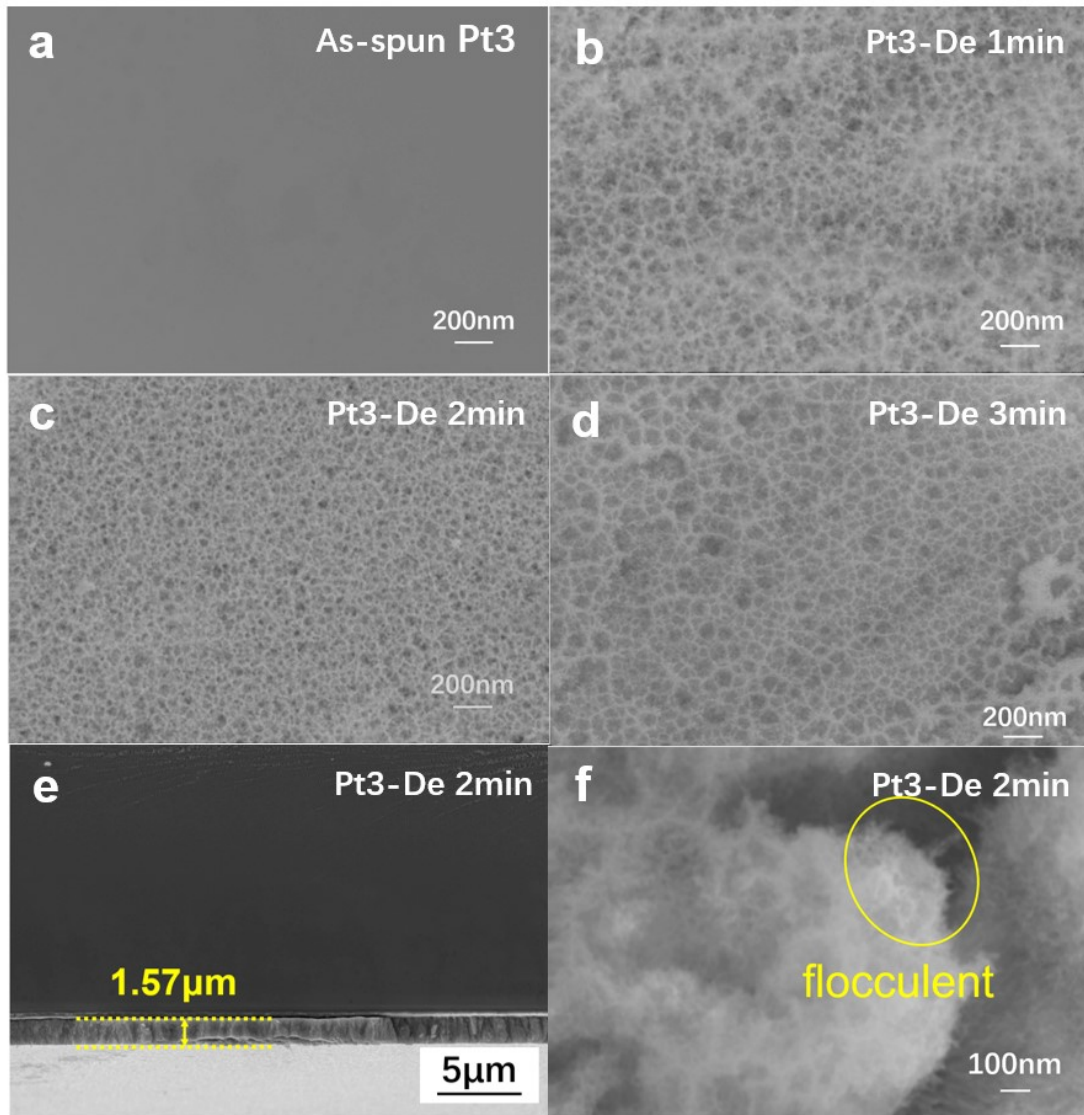
**Fig. S3** SEM structure and morphology of the $Fe_{70-x}Co_{10}Ni_{10}Zr_{10}Pt_x$ ($x$=3) series samples. (a) The image of the as-spun Pt3 ribbon with smooth surface. (b-d) Surface morphology images of the as-spun Pt3 ribbon after 1 minute, 2 minutes, 3 minutes of dealloying with nanopourous surface (Pt3-De 1min, 2min, 3min). (e) Cross-section morphology of Pt3-De 2min ribbon, the thickness of the nanoporous layer is 1.5μm. (f) The flocculent cross-section of the nanoporous layer of Pt3-De 2min sample.

(The sample of Pt3-De 2 min is named Pt3/MG)
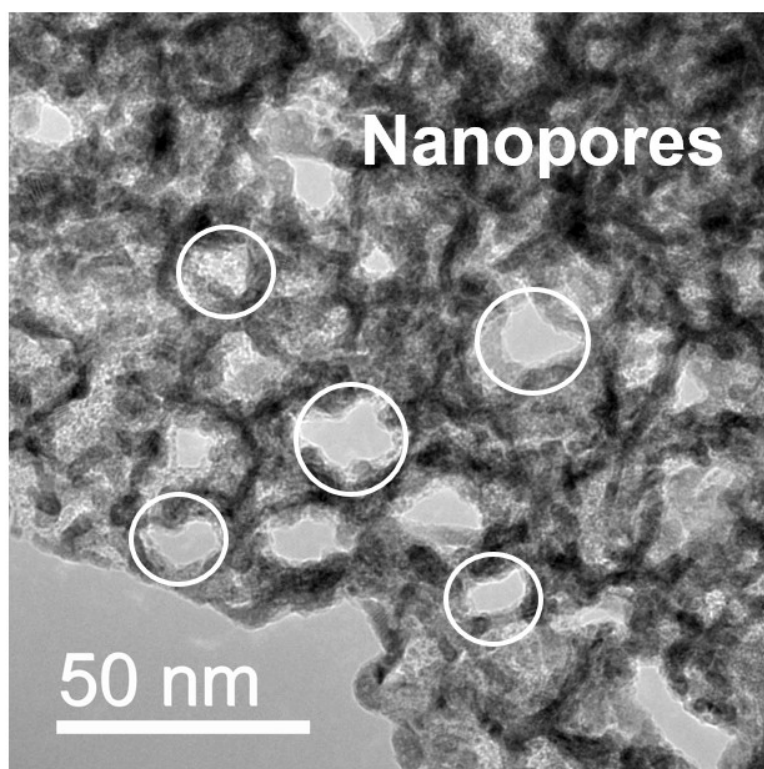
**Fig. S4** The high-resolution transmission electron micrographs (HRTEM) of nanoporous surfaces of Pt3/MG.
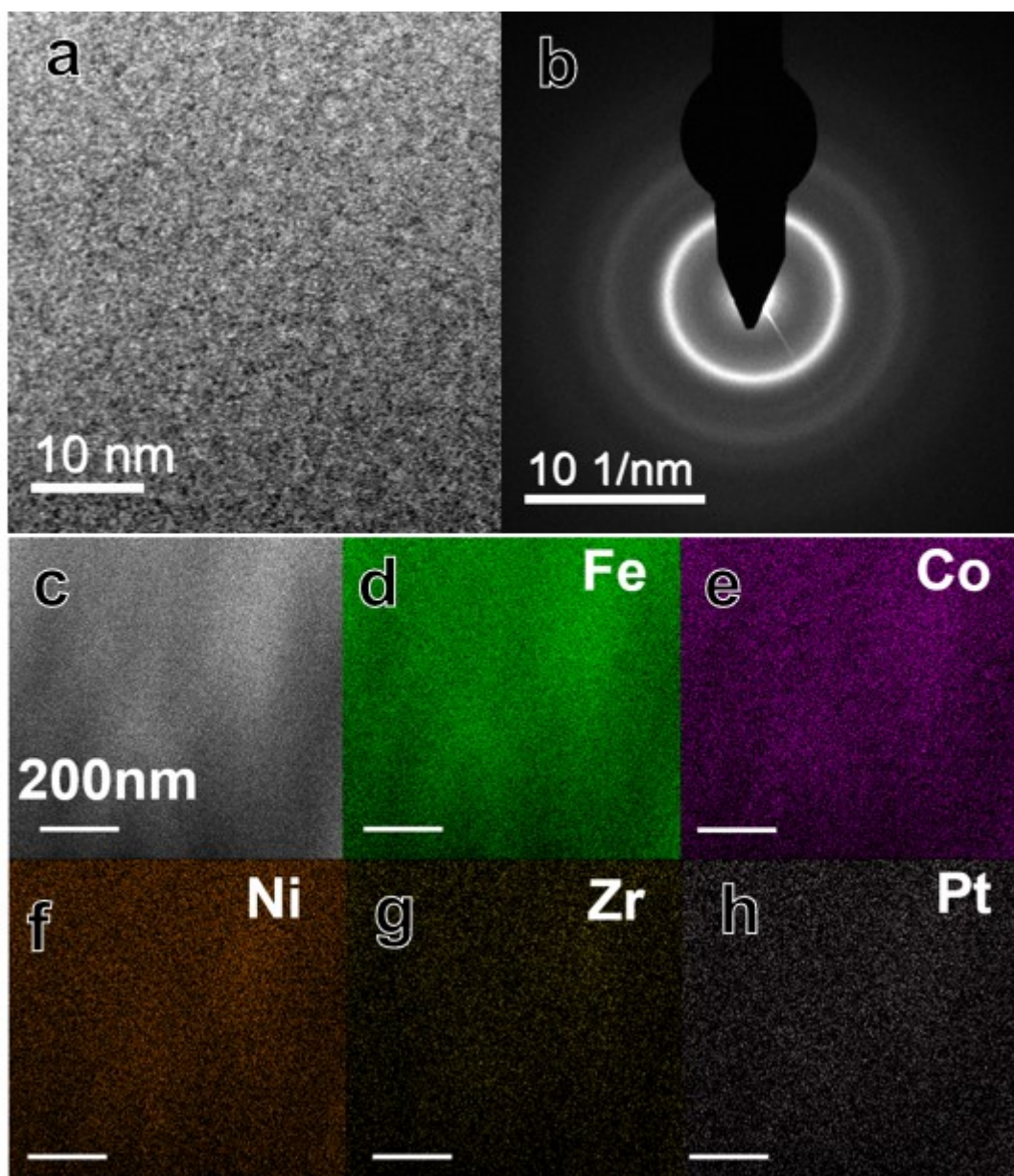
**Fig. S5** Structural analysis of as-spun Pt3 ribbon. (a) The HRTEM image of the ribbon. (b) SAED image of the ribbon demonstrate the sample is the metallic glass. (c-h) STEM-EDS mapping images of the as-spun Pt3.
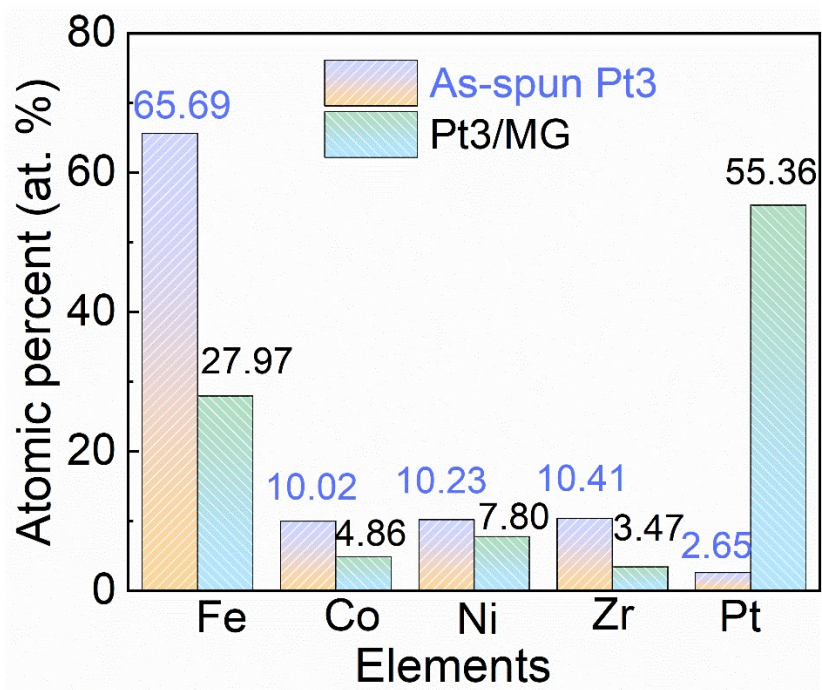
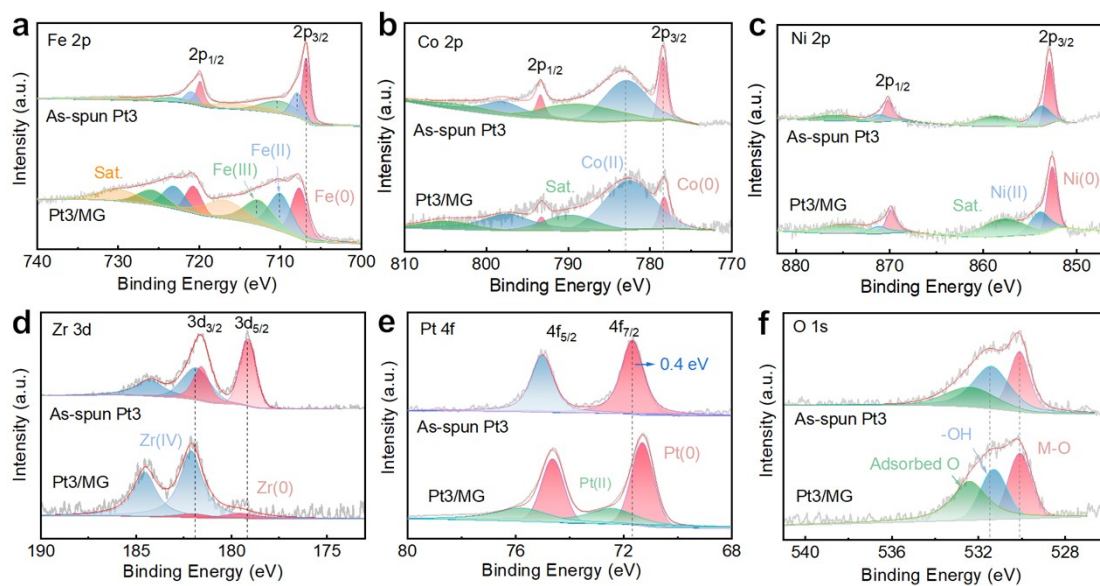**Fig. S6** EDS results of the as-spun Pt3 and Pt3/MG catalyst.

**Fig. S7** High-resolution XPS spectra of the as-spun Pt3 and Pt3/MG catalyst. (a) Fe 2p, (b) Co 2p, (c) Ni 2p, (d) Zr 3d, (e) Pt 4f, and (f) O 1s.
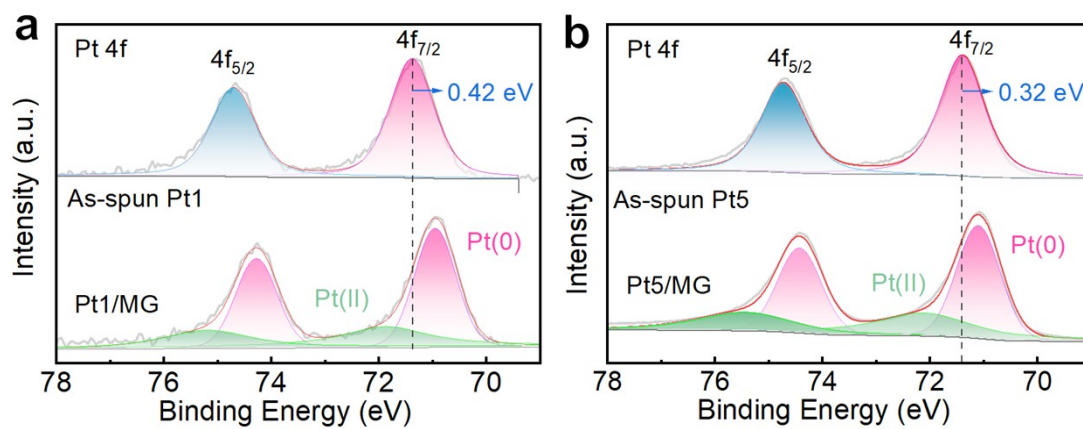
**Fig. S8** XPS spectrum of the catalysts taken at Pt 4*f*. (a) Pt 4f of as-spun Pt1 and Pt1/MG catalysts, (b) Pt 4f of as-spun Pt5 and Pt5/MG catalysts.
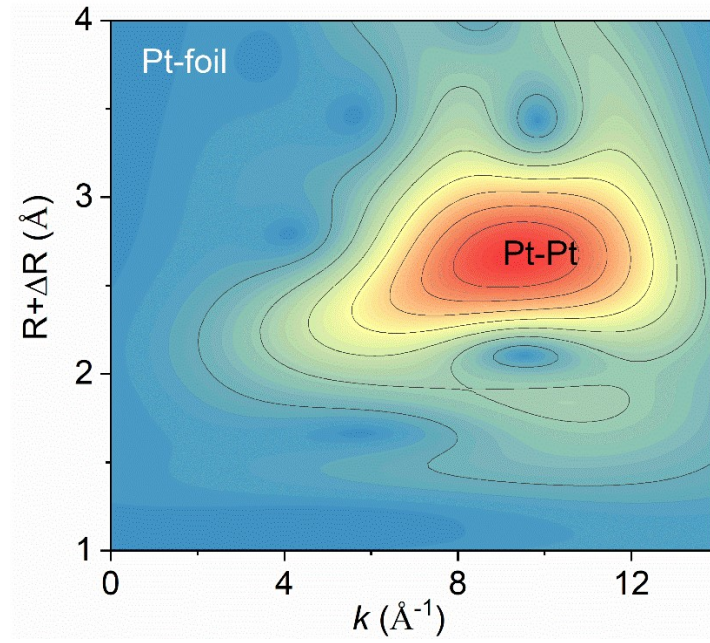
**Fig. S9** Wavelet transform (WT) images for the (FT) $k^3$ weighted $\chi(k)$-function of Pt foil.
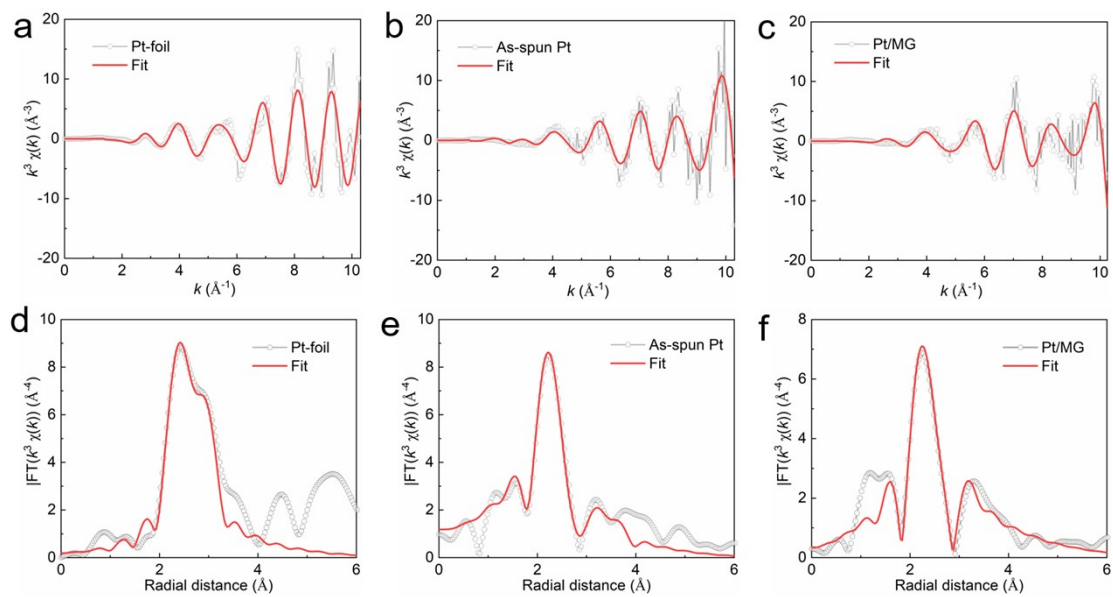
**Fig. S10** The raw data and corresponding EXAFS fitting curves of Pt L3-edge. (a,d) Pt-foil, (b,e) as-spun Pt, and (c,f) Pt/MG.
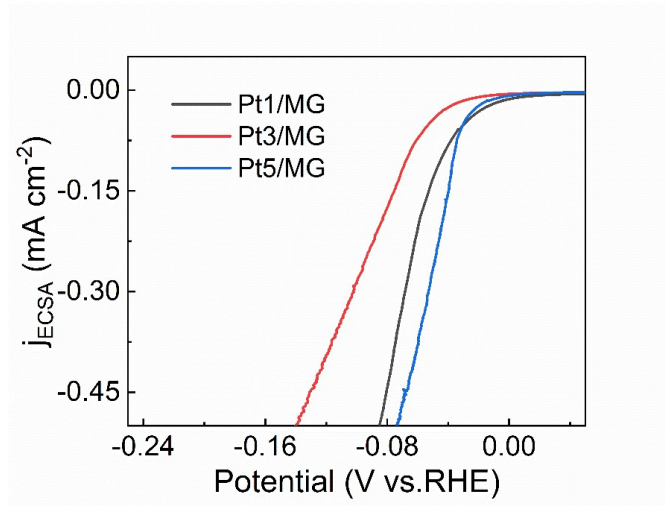
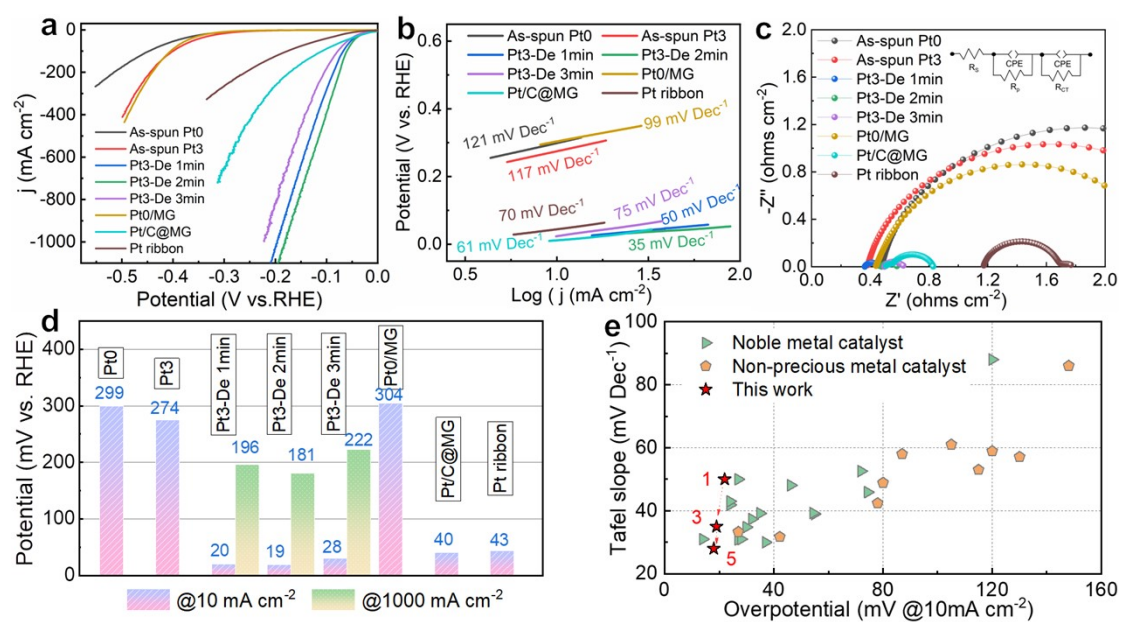**Fig. S11** Normalized linear sweep voltammetry (LSV) curve based on the electrochemically active surface area (ECSA) of Pt*x*/MG

**Fig. S12** Electrochemical properties in an alkaline 1 M KOH solution for $Fe_{67}Co_{10}Ni_{10}Zr_{10}Pt_3$ (as-spun Pt3) and its dealloying ribbons (dealloying for 1-3 minutes). (a) HER polarization curves of the ribbons. (b) The corresponding Tafel slopes. (c) Nyquist plots of the ribbons. (d) Comparision of the overpotential of the tested samples. (e) Comparison of HER activity with recently reported electrocatalysts.

(The sample of Pt3-De 2 min is named asPt3/MG)
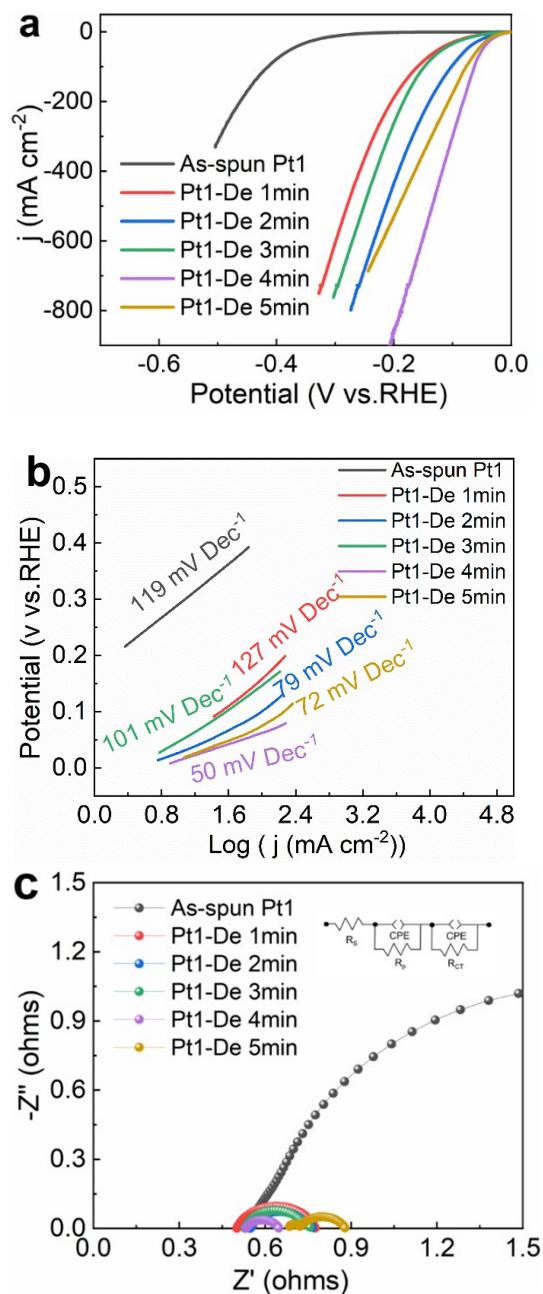
**Fig. S13** Electrochemical properties in an alkaline 1 M KOH solution for $Fe_{67}Co_{10}Ni_{10}Zr_{10}Pt_3$ (as-spun Pt1) and its dealloyed ribbons (dealloying for 1-5 minutes). (a) HER polarization curves of the ribbons. (b) The corresponding Tafel slopes. (c) Nyquist plots of the ribbons.

(The sample of Pt1-De 4 min is named as Pt1/MG)

**Fig. S14** Electrochemical properties in an alkaline 1 M KOH solution for $Fe_{65}Co_{10}Ni_{10}Zr_{10}Pt_5$ (as-spun Pt5) and its dealloying ribbons (dealloying for 1-4 minutes). (a) HER polarization curves of the ribbons. (b) The corresponding Tafel slopes. (c) Nyquist plots of the ribbons.

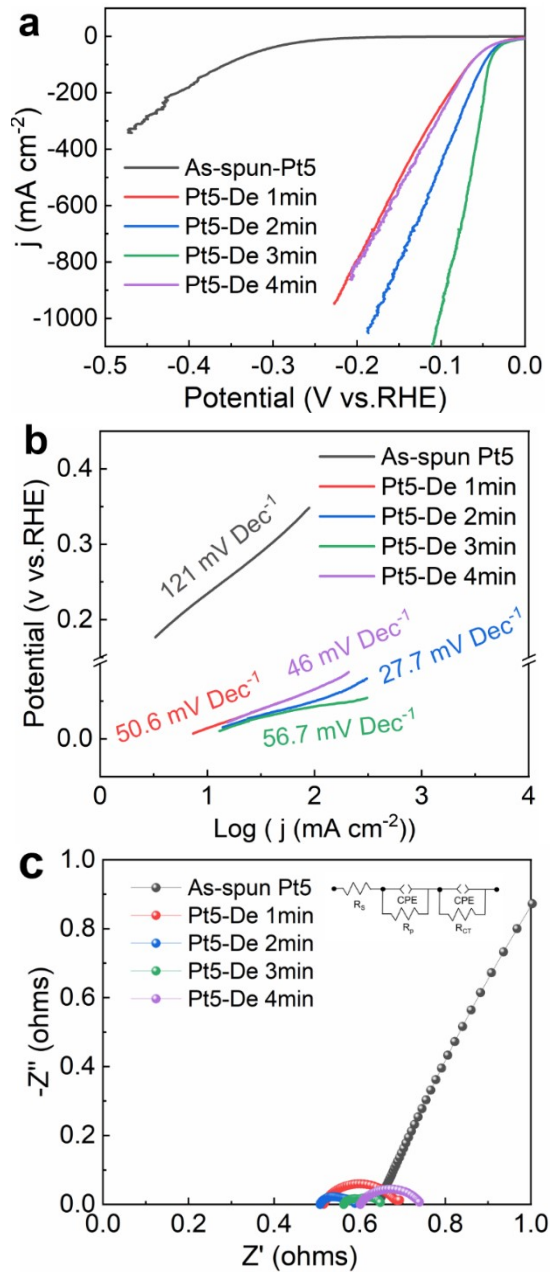(The sample of Pt5-De 3 min is named as Pt5/MG)
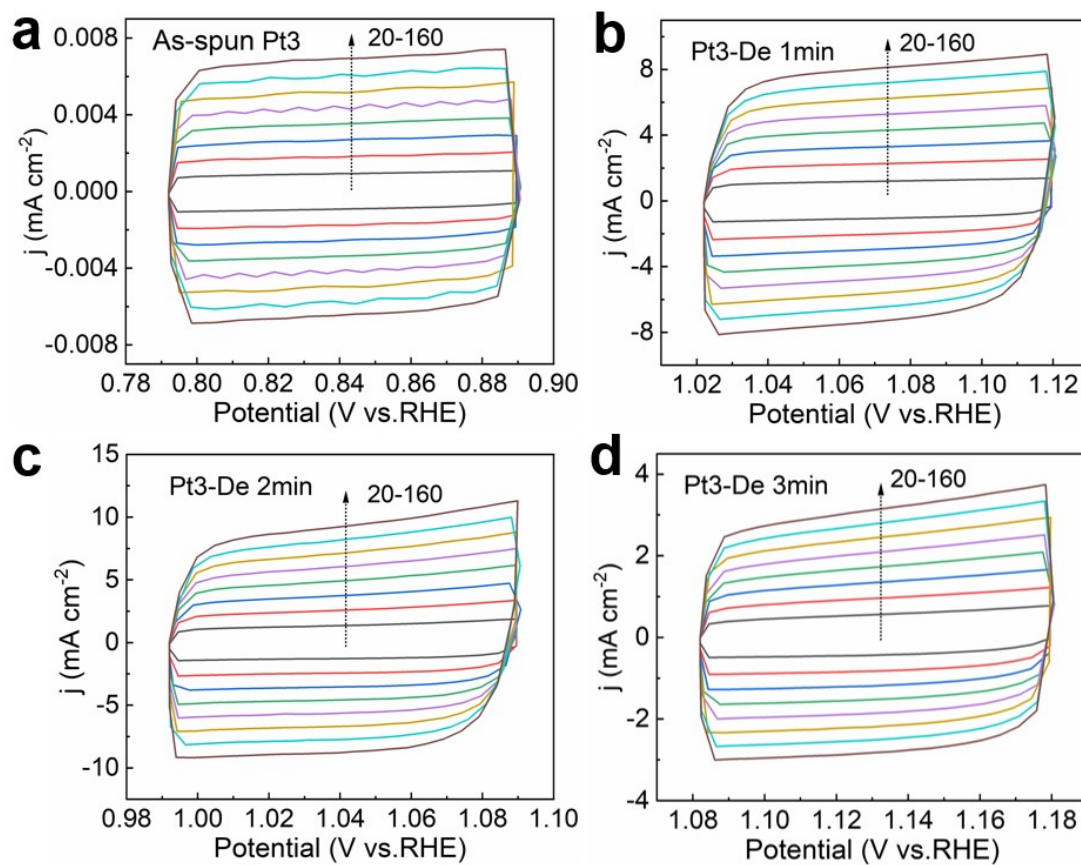
**Fig. S15** Cyclic voltammogram (CV) curves in 1 M KOH for. (a) As-spun Pt3. (b) Pt3-De 1min. (c) Pt3-De 2min. (d) Pt3-De 3min. (The curves were performed at various scan rates (20, 40, 60, 80, 100,120,140 and 160 mV s$^{-1}$).
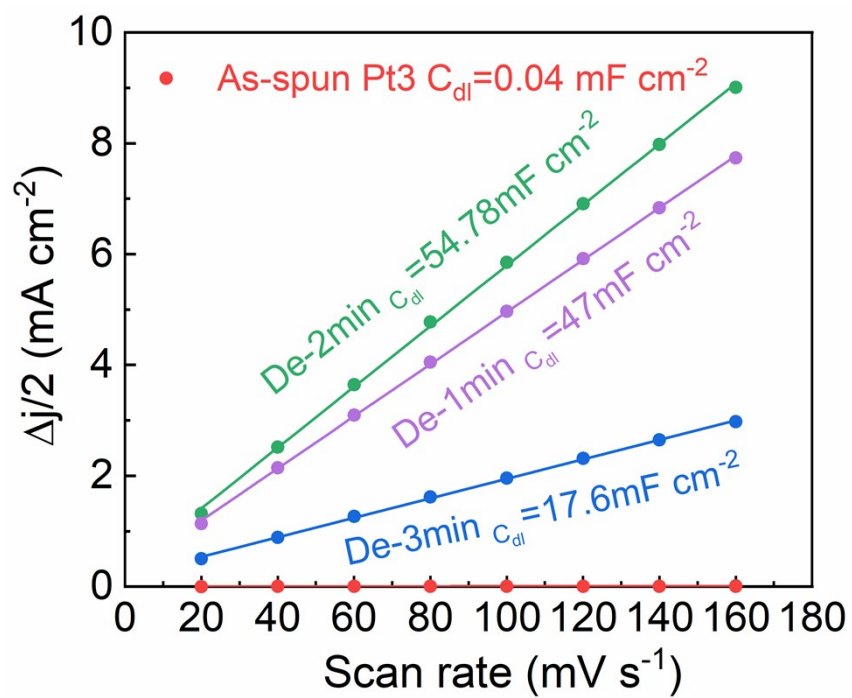
**Fig. S16** The measured capacitive currents plotted as a function of scan rate.
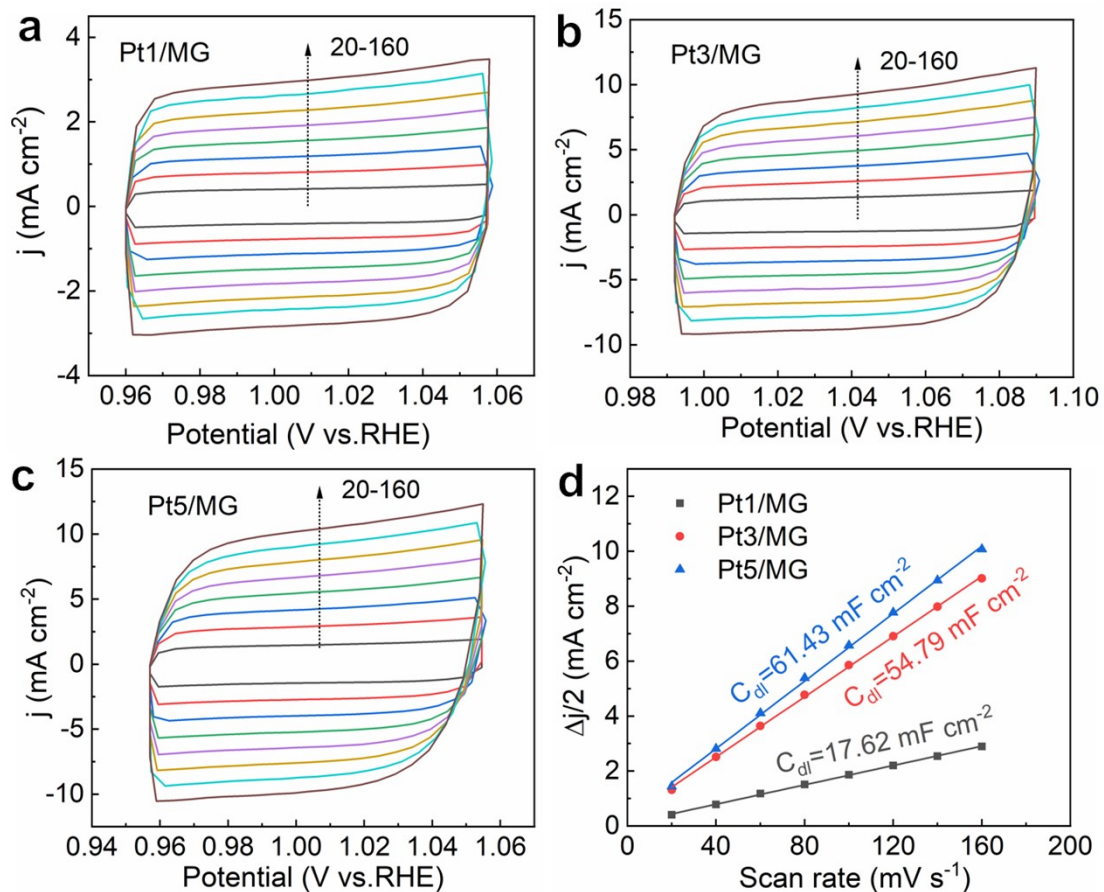
**Fig. S17** Cyclic voltammogram (CV) curves in 1 M KOH for ((a) Pt1/MG catalyst. (b) Pt3/MG catalyst. (c) Pt5/MG catalyst. (d) Pt3-De 3min. (d) Capacitive current as a function of scan rates.
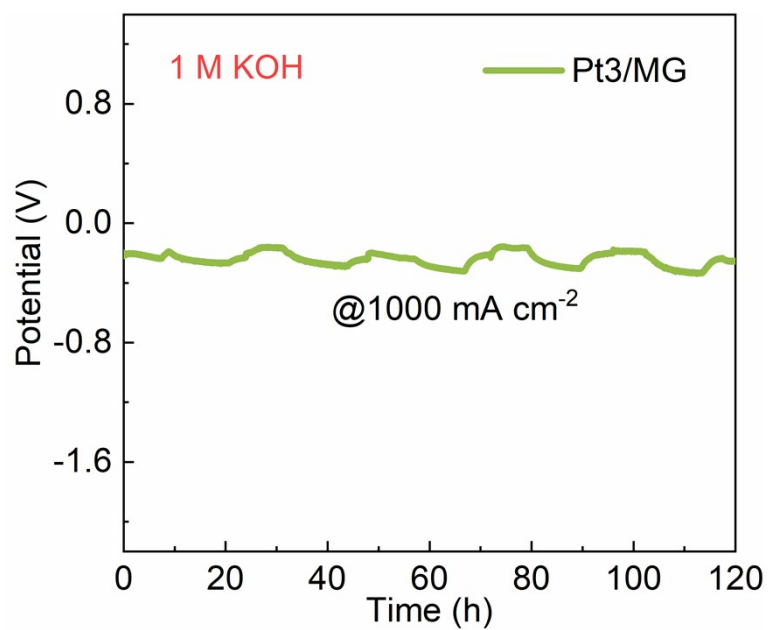
**Fig. S18** Long-term stability test of Pt3/MG at a current density of 1000 mA cm$^{-2}$ for 120 h.
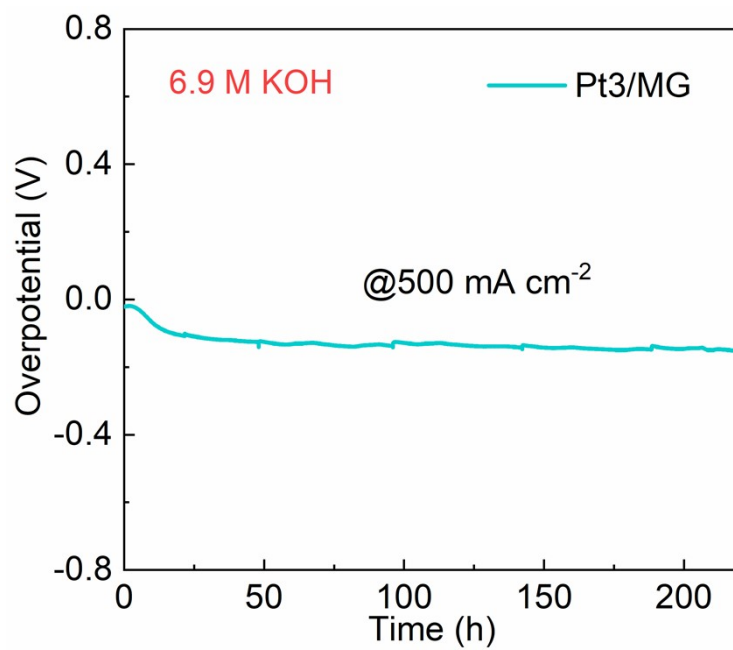
**Fig. S19** Long-term stability test of Pt3/MG at a current density of 500 mA cm$^{-2}$ for 220 h at 6.9 M KOH condition.
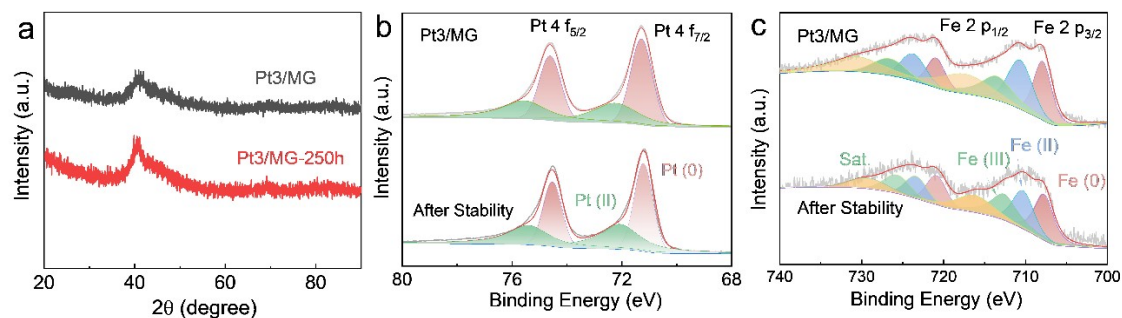
**Fig. S20** (a) The XRD pattern of the Pt3/MG after a stability test of 250 hours for the Pt3/MG. (b) The XPS spectra of the Pt 4f after a stability test of 250 hours for the Pt3/MG. (c) The XPS spectra of the Fe 2p after a stability test of 250 hours for the Pt3/MG.
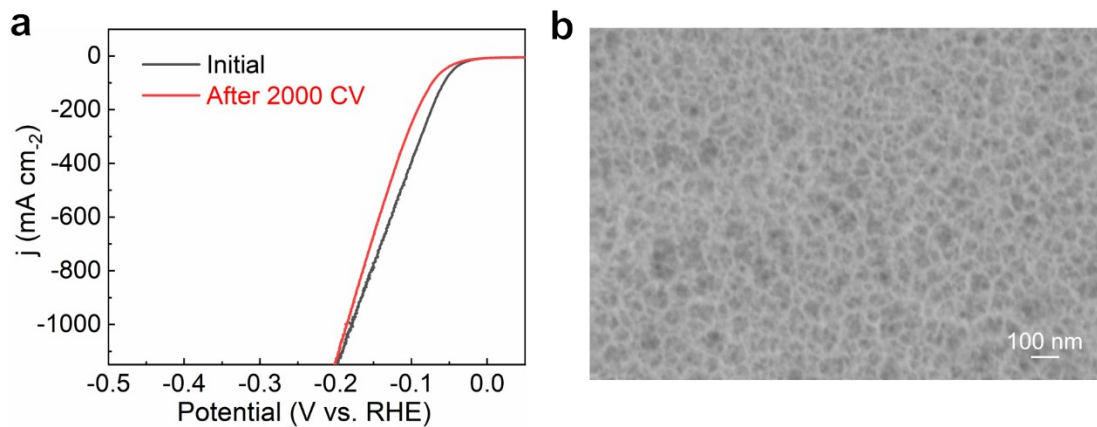
**Fig. S21** (a) Comparison of polarization curves of Pt3/MG catalyst after 2000 CV cycles. (b) The SEM image of chronopotentiometry stability test over 80 h at a constant current density of 500 mA cm$^{-2}$.
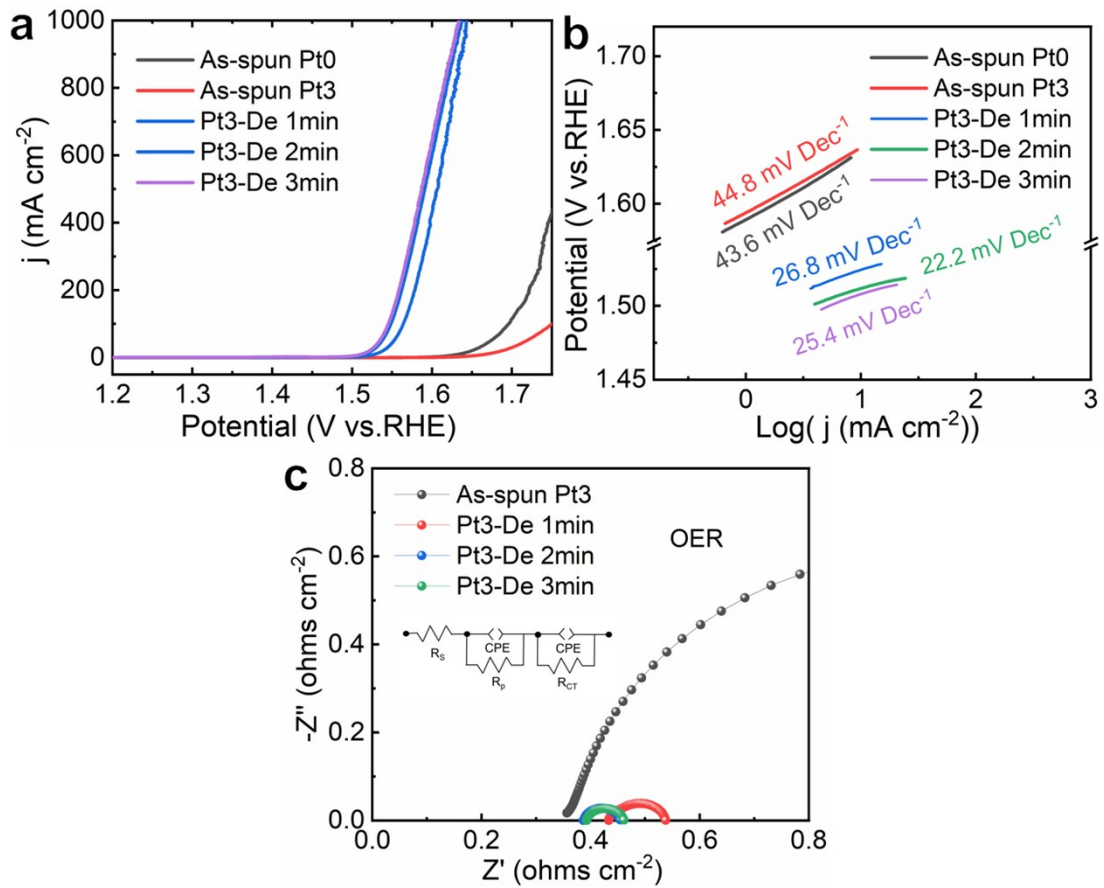
**Fig. S22** Electrochemical properties in an alkaline 1 M KOH solution. (a) OER polarization curves of the ribbons. (b) The corresponding Tafel slopes. (c) Nyquist plots of the ribbons.
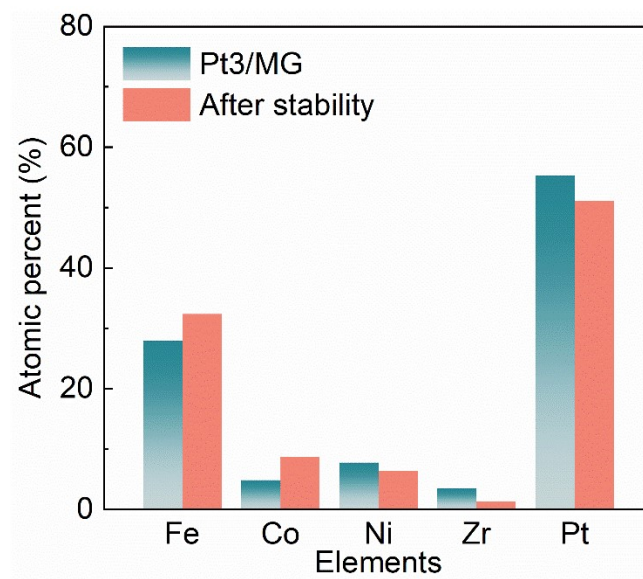
**Fig. S23** EDS elemental content of Pt3/MG catalyst samples before and after the stability test.
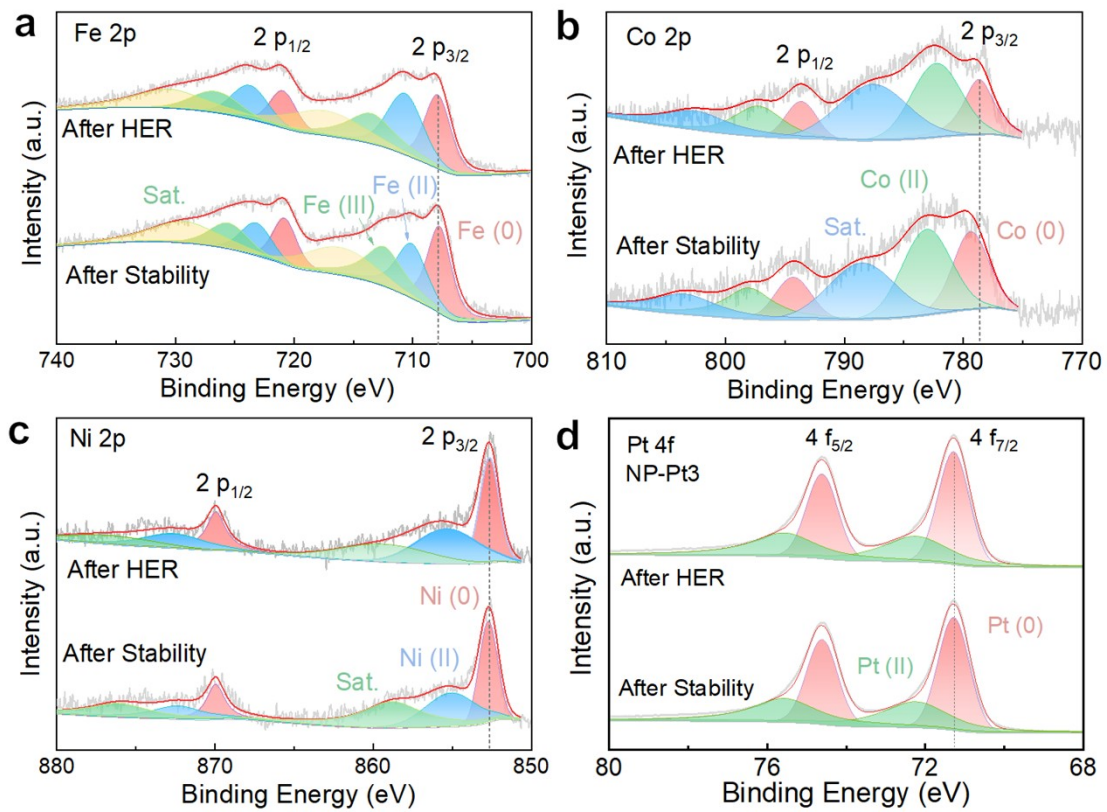
**Fig. S24** High-resolution XPS spectra of the Pt3/MG catalyst after HER test and stability test. (a) Fe 2p, (b) Co 2p, (c) Ni 2p and (d) Pt 4f.
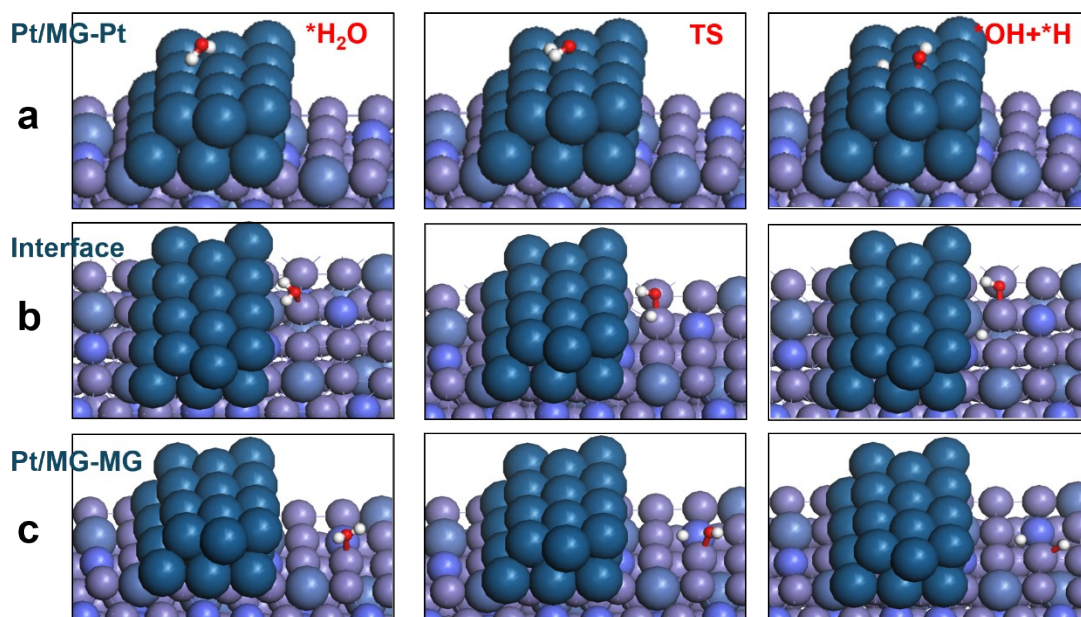
**Fig. S25** The search for transition states and diagrams of the water dissociation process at three distinct sites. (a) Pt/MG-Pt, (b) Pt/MG-interface and (c) Pt/MG-MG.

**Table S1.** EXAFS fitting parameters at the Pt L3-edge for various samples. ($S_0^2 = 0.83$)

| Sample | Path | CN | R(Å) | $\sigma^2$(Å$^2$) | $\Delta E_0$ |
|--------|------|-----|------|----------|------|
| Pt-foil | Pt-Pt | 12 | 2.78 | 0.005 | 7.33 |
| As-spun Pt | Pt-Pt | 5.68 | 3.58 | 0.014 | 4.92 |
| | Pt-Fe/Co/Ni | 4.11 | 2.62 | 0.009 | |
| | Pt-Zr | 0.001 | 2.10 | 0.034 | |
| Pt/MG | Pt-Pt | 7.361 | 2.844 | 0.0016 | 2.16 |
| | Pt-Fe/Co/Ni | 1.591 | 2.525 | 0.0045 | |

(CN: coordination number; R: the distance to the neighboring atom; $\sigma^2$: the Mean Square Relative Displacement (MSRD); $\Delta E_0$: inner potsential correction; R factor indicates the goodness of the fit.

$S_0^2$ was fixed to 0.83, according to the experimental EXAFS fit of Pt-foil by fixing CN as the known crystallographic value.

Fitting range: $3.0 \leq k$ (Å$^{-1}$)$\leq 10.3, 1.0 \leq R$ (Å)$\leq 3.0$ (Pt-foil); $3.0 \leq k$ (Å$^{-1}$) $\leq 10.3$ and $1.0 \leq R$ (Å) $\leq 4.0$ (As-spun Pt); $3.0 \leq k$ (Å$^{-1}$) $\leq 10.3$ and $1.0 \leq R$ (Å) $\leq 3.0$ (Pt/MG).)

**Table S2.** The overpotential data for Pt*x*/MG at current densities of 10 mA cm$^{-2}$ and 1000 mA cm$^{-2}$

| j \ Electrocatalysts | Pt1/MG (mV) | Pt3/MG (mV) | Pt5/MG (mV) |
|---|---|---|---|
| 10 mA cm$^{-2}$ | 22 | 19 | 18 |
| 1000 mA cm$^{-2}$ | / | 181 | 102 |

**Table S3.** Comparison of HER overpotentials ($\eta$) at 10 mA cm$^{-2}$ of different electrocatalysts in 1 M KOH solution.

| Electrocatalysts | $\eta$10 (mV) | Tafel (mV Dec$^{-1}$) | Refs. |
|---|---|---|---|
| Pt1/MG (This work) | 22 | 50 | |
| Pt3/MG (This work) | 19 | 35 | |
| Pt5/MG (This work) | 18 | 27.7 | |
| Pt/C$_{60}$ | 24 | 41.9 | [5] |
| AlMnYNiCoCu | 124 | 69 | [6] |
| NiMo-65 | 17 | 28 | [7] |
| NS-AlNiCoMnYAu | 24 | 43 | [8] |
| FeCoNiBPt | 27 | 30.9 | [9] |
| Ni(NPN)/MG | 78 | 42.4 | [10] |
| NiCoP/NPC | 80 | 48.9 | [11] |
| Cu@WC | 119 | 50.5 | [12] |
| Ni(Cu)/NF | 27 | 33.3 | [13] |
| Ni$_4$Mo/CF | 128 | 33.2 | [14] |
| Np-NiZrTiPt | 37 | 30 | [15] |
| FeCoNiCu | 42.2 | 31.7 | [16] |
| PdPtCuNiP-HEMG | 32 | 37.4 | [17] |
| Pt/np-Co$_{0.85}$Se | 55 | 39 | [18] |
| np-Co$_{0.85}$Se | 264 | 90 | [18] |
| PtNiP MNs/C | 54.4 | 39.3 | [19] |
| PtNi MNs/C | 74.4 | 45.9 | [19] |

**Table S3.** Comparison of HER overpotentials ($\eta$) at 10 mA cm$^{-2}$ of different electrocatalysts in 1 M KOH solution. (continue)

| Electrocatalysts | $\eta10$ (mV) | Tafel (mV Dec$^{-1}$) | Refs. |
|---|---|---|---|
| PtP MNs/C | 72.0 | 52.6 | [19] |
| Np-NiZrTiPt | 37 | 30 | [15] |
| FePO$_4$/NF | 123 | 104.49 | [20] |
| Ni(NPN)/MG | 78 | 42.4 | [10] |
| Ru$_{0.48}$Re$_{0.52}$NPs@rGO | 14 | 31 | [21] |
| NiCo$_2$Px | 63 | 34.4 | [22] |
| Ir/CNT/rGO | 19 | 32 | [23] |
| Ir/CNT | 35 | 39.2 | [24] |
| Ir/rGO | 30 | 34.8 | [25] |
| Ni-MOF@Pt | 120 | 88 | [26] |
| IrNi@GO | 27 | 50 | [22] |
| Pt@CoS | 28 | 31 | [27] |
| Pt/HMCS | 46.2 | 48.1 | [24] |
| Ptc/Ni(O(H)$_2$/PN | 32 | 86 | [28] |
| Ni$_{0.5}$Co$_{0.5}$P | 87 | 58 | [29] |
| Cu@NiFe LDH | 120 | 58.9 | [27] |
| WN NW | 130 | 57.1 | [30] |
| Ni$_3$FeN | 105 | 61 | [31] |
| CoP/NCNHP | 115 | 53 | [32] |
| Co/HCNHP | 168 | 101 | [32] |
| CoP/NCP | 148 | 86 | [32] |

**Table S4.** Comparison of HER overpotentials ($\eta$) at 1000 mA cm$^{-2}$ of different electrocatalysts in 1 M KOH solution

| Electrocatalysts | $\eta 1000$ (mV) | Refs. |
|---|---|---|
| Pt3/MG | 181 | |
| Pt5/MG | 102 | |
| $MoS_2/Ni_3S_2/NF$ | 200 | [33] |
| $Sr_2RuO_4$ | 278 | [34] |
| $F\text{-}Co_2P/Fe_2P/IF$ | 292 | [35] |
| $Ni_{2(1-x)}Mo_{2x}P$ | 294 | [35] |
| A-NiCo LDH/NF | 381 | [36] |
| $HC\text{-}MoS_2/Mo_2C$ | 412 | [37] |

**Table S5.** Summary of various catalysts for TOF in alkaline condition

| Electrocatalysts | Overpotential(mV) | TOF (H2 S-1) | Reference |
|---|---|---|---|
| NiFeCoCuTi | 200 | 0.812 | 38 |
| Pt/C$_{60}$ | 100 | 17.6 | 5 |
| Pt/C | 100 | 1.5 | 5 |
| np-PdPtCuNiP | 50 | 6.58 | 17 |
| np-Co$_{0.85}$Se | 100 | 0.17 | 18 |
| Pt/np- Co$_{0.85}$Se | 100 | 3.93 | 18 |
| NiZrTiPt | 100 | 0.89 | 15 |
| Pt/C | 100 | 0.49 | 15 |
| Np-AlMnYNiCoAu$_3$ | 150 | 0.94 | 6 |
|  | 200 | 2.7 | 6 |
| MoS$_3$ | 200 | 0.3 | 39 |

Table S6. ICP test results of the solution after the dealloying process and stability test of the sample Pt3/MG.

| Element | Fe (mg/L) | Co (mg/L) | Ni (mg/L) | Zr (mg/L) | Pt (mg/L) |
|---|---|---|---|---|---|
| Dealloying process | 91.84 | 14.79 | 14.42 | 7.04 | <0.05 |
| Stability test | <0.05 | <0.05 | <0.05 | <0.05 | <0.05 |

Table S7. $\Delta G_{*H}$ of the Pt/MG and Pt (111).

| Sites | Pt (111) | Pt/MG-Pt-top | Pt/MG-Pt-bridge | Pt/MG-Pt-hole | Pt/MG-MG | Pt/MG-interface |
|---|---|---|---|---|---|---|
| $\Delta G_{*H}$ (eV) | -0.11 | -0.46 | -0.83 | -0.21 | -0.42 | -0.86 |

# References

1. Q. Yang, G. Li, K. Manna, F. Fan, C. Felser and Y. Sun, *Adv. Mater.*, 2020, **32**, 1908518.

2. B. Delley, *J. Chem. Phys.*, 2000, **113**, 7756-7764.

3. J. P. Perdew, K. Burke and M. Ernzerhof, *Phys. Rev. Lett.*, 1996, **77**, 3865-3868.

4. M. Methfessel and A. T. Paxton, *Phys. Rev. B*, 1989, **40**, 3616-3621.

5. J. Chen, M. Aliasgar, F. B. Zamudio, T. Zhang, Y. Zhao, X. Lian, L. Wen, H. Yang, W. Sun, S. M. Kozlov, W. Chen and L. Wang, *Nat. Commun.*, 2023, **14**, 1711.

6. P. Zou, B. Zang, L. Song, W. Xu, J. Huo and J.-Q. Wang, *ACS Appl. Nano Mater.*, 2022, **5**, 17673-17681.

7. A. Nairan, P. Zou, C. Liang, J. Liu, D. Wu, P. Liu and C. Yang, *Adv. Funct. Mater.*, 2019, **29**, 1903747.

8. X. Liu, S. Ju, P. Zou, L. Song, W. Xu, J. Huo, J. Yi, G. Wang and J.-Q. Wang, *J. Alloys Compd.*, 2021, **880**, 160548.

9. X. Zhang, Y. Yang, Y. Liu, Z. Jia, Q. Wang, L. Sun, L. C. Zhang, J. J. Kruzic, J. Lu and B. Shen, *Adv. Mater.*, 2023, **35**, 2303439.

10. J. Wang, L. You, Z. Li, X. Liu, R. Li, Q. Du, X. Wang, H. Wang, Y. Wu, S. Jiang and Z. Lu, *J Mater. Sci. Technol.*, 2021, **73**, 145-150.

11. Z. B. Li, J. Wang, X. J. Liu, R. Li, H. Wang, Y. Wu, X. Z. Wang and Z. P. Lu, *Scripta Mater.*, 2019, **173**, 51-55.

12. M. Yao, B. Wang, B. Sun, L. Luo, Y. Chen, J. Wang, N. Wang, S. Komarneni, X. Niu and W. Hu, *Appl. Catal B-Environ.*, 2021, **280**, 119451.

13. Q. Sun, Y. Dong, Z. Wang, S. Yin and C. Zhao, *Small*, 2018, **14**, e1704137.

14. S. Feng, J. Wang, W. Wang, X. Wang, Y. Zhang, Chenchen, A. Ju, J. Pan and R. Xu, *Adv. Mat. Interfaces*, 2021, **8**. 2100500

15. R. Li, X. Liu, R. Wu, J. Wang, Z. Li, K. C. Chan, H. Wang, Y. Wu and Z. Lu, *Adv. Mater.*, 2019, **31**, e1904989.

16. R. Li, X. Liu, W. Liu, Z. Li, K. C. Chan and Z. Lu, *Adv Sci (Weinh)*, 2022, **9**, e2105808.

17. Z. Jia, K. Nomoto, Q. Wang, C. Kong, L. Sun, L. C. Zhang, S. X. Liang, J. Lu and J. J. Kruzic, *Adv. Funct. Mater.*, 2021, **31**, 2101586.

18. K. Jiang, B. Liu, M. Luo, S. Ning, M. Peng, Y. Zhao, Y.-R. Lu, T.-S. Chan, F. M. F. de Groot

and Y. Tan, *Nat. Commun.*, 2019, **10**, 1743.

19. C. Li, Y. Xu, D. Yang, X. Qian, X. Chai, Z. Wang, X. Li, L. Wang and H. Wang, *ACS Sustainable Chem. Eng.*, 2019, **7**, 9709-9716.

20. L. Yang, Z. Guo, J. Huang, Y. Xi, R. Gao, G. Su, W. Wang, L. Cao and B. Dong, *Adv. Mater.*, 2017, **29**, 1704574.

21. S. Y. Xu, P. Zhang, Z. Y. Li, C. H. Chung, M. W. Moon, J. M. Kim and P. J. Yoo, *Appl. Surf. Sci.*, 2023, **638**.

22. R. Zhang, X. Wang, S. Yu, T. Wen, X. Zhu, F. Yang, X. Sun, X. Wang and W. Hu, *Adv. Mater.*, 2016, **29**, 1605502.

23. B. Huang, Y. Ma, Z. Xiong, W. Lu, R. Ding, T. Li, P. Jiang and M. Liang, *Sustain. Energ. Fuels*, 2020, **4**, 3288-3292.

24. K. Rui, G. Zhao, M. Lao, P. Cui, X. Zheng, X. Zheng, J. Zhu, W. Huang, S. X. Dou and W. Sun, *Nano Letters*, 2019, **19**, 8447-8453.

25. S. Gong, C. Wang, P. Jiang, K. Yang, J. Lu, M. Huang, S. Chen, J. Wang and Q. Chen, *J. Mater. Chem. A*, 2019, **7**, 15079-15088.

26. A. Mosallanezhad, C. Wei, P. Ahmadian Koudakan, Y. Fang, S. Niu, Z. Bian, B. Liu, T. Huang, H. Pan and G. Wang, *Appl. Catal B-Environ.*, 2022, **315**, 121534.

27. X. K. Wan, H. B. Wu, B. Y. Guan, D. Luan and X. W. Lou, *Adv. Mater.*, 2019, **32**, 1901349.

28. B. Ruqia and S. I. Choi, *ChemSusChem*, 2018, **11**, 2643-2653.

29. Y. Li, Z. Jiang, J. Huang, X. Zhang and J. Chen, *Electrochim. Acta*, 2017, **249**, 301-307.

30. B. Ren, D. Li, Q. Jin, H. Cui and C. Wang, *J. Mater. Chem. A*, 2017, **5**, 19072-19078.

31. Z. Liu, H. Tan, J. Xin, J. Duan, X. Su, P. Hao, J. Xie, J. Zhan, J. Zhang, J.-J. Wang and H. Liu, *Acs Appl. Mater. Inter.*, 2018, **10**, 3699-3706.

32. Y. Pan, K. Sun, S. Liu, X. Cao, K. Wu, W.-C. Cheong, Z. Chen, Y. Wang, Y. Li, Y. Liu, D. Wang, Q. Peng, C. Chen and Y. Li, *J. Am. Chem. Soc.*, 2018, **140**, 2610-2618.

33. H. Wang, M. Zhou, P. Choudhury and H. Luo, *Applied Materials Today*, 2019, **16**, 56.

34. Y. Zhang, K. E. Arpino, Q. Yang, N. Kikugawa, D. A. Sokolov, C. W. Hicks, J. Liu, C. Felser and G. Li, *Nat Commun*, 2022, **13**, 7784.

35. X.-Y. Zhang, Y.-R. Zhu, Y. Chen, S.-Y. Dou, X.-Y. Chen, B. Dong, B.-Y. Guo, D.-P. Liu, C.-G. Liu and Y.-M. Chai, *Chem. Eng. J.*, 2020, **399**, 125831.

36. H. Wang and L. Gao, *Curr. Opin. Electroche.*, 2018, **7**, 2185-2191.

37. C. Zhang, Y. T. Luo, J. Y. Tan, Q. M. Yu, F. N. Yang, Z. Y. Zhang, L. S. Yang, H. M. Cheng and B. L. Liu, *Nat. Commun.*, 2020, **11**, 3724.

38. H. Shi, X.-Y. Sun, S.-P. Zeng, Y. Liu, G.-F. Han, T.-H. Wang, Z. Wen, Q.-R. Fang, X.-Y. Lang and Q. Jiang, *Small Struct.*, 2023, **4**, 2300042.

39. J. D. Benck, Z. Chen, L. Y. Kuritzky, A. J. Forman and T. F. Jaramillo, *ACS Catal.*, 2012, **2**, 1916-1923.